Quantum Information and Computation, Vol. 7, No. 1 (2007) 052–072


# MODELING ION TRAP THERMAL NOISE DECOHERENCE

DAVID LEIBRANDT [a], BERNARD YURKE and RICHART SLUSHER
*Lucent Technologies, Bell Laboratories*
*Murray Hill, NJ 07974, USA*

Received January 14, 2006
Revised April 24, 2006

We present a detailed analysis of ion heating caused by thermal fluctuation noise in ion traps. The results of the analysis are used to estimate thermal noise ion heating rates for a variety of trap electrode configurations and materials, including recent scalable multiplexed planar ion trap proposals based on silicon VLSI technology. We find that minimizing thermal noise ion heating places severe constraints on the design and materials used for ion traps.

*Keywords*: ion traps, decoherence, quantum computing

*Communicated by*: D Wineland & R Blatt

## 1 Introduction

Trapped ions are a promising technology for achieving quantum computation. There is hope that quantum computers will provide unique speedup and regeneration artibutes relative to classical computers for a limited range of tasks including factoring large numbers, searching large data bases, simulating large quantum systems, and regenerating quantum cryptographic signals. The hyperfine or metastable ion levels are used as qubits. Single qubit operations are achieved by laser excitation pulses on single ions. Two qubit operations make use of the vibrational or motional coupling between the ions. These two qubit operations are sensitive to random vibrational excitations of the ion motion in the trap. Ideally the ions are Doppler and Raman sideband cooled to their lowest vibrational level and kept cold throughout the quantum computation. Vibrational level spacings are at frequencies of a few megahertz. It is also preferable to operate the computer with the trapping and control electrodes at room temperature. However, in a room temperature environment, thermal fluctuations in the resistive elements of the electrodes and voltage supplies will inevitably heat the ions and constitute a fundamental limit for decoherence errors introduced by ion heating. The thermal fluctuation heating has not been a primary concern for experiments to date since the ions are far enough from the electrodes to make the thermal fluctuation heating rates fall into the range below one motional quanta per second, much smaller than the heating rates actually observed which are thought to be caused by patch potential fluctuations on the electrode surfaces. However, as the dimensions of the trap electrodes are reduced to achieve scalable

[a]Present address: Department of Physics, Massachusetts Institute of Technology, Cambridge, MA 02139

quantum computers, the thermal heating constraints should be taken into account in the trap design process.

Thermal fluctuation heating can be thought of as arising from voltages generated by thermal electrical currents in the resistive elements of the trap circuit. Analysis shows that the ion heating rates from these fluctuating thermal potentials vary as the inverse square of the distance between the electrode and the ion and directly with the resistance in the circuit. The symmetry of the trapping electrodes is also important in determining the ion heating rates. We find from the analysis presented here that the ion heating rates can become a major concern as ion trap designs evolve towards scalable multiplexed ion trapping systems, new electrode materials, more complex electrode configurations, and ion transport between a variety of trap locations. We present an in-depth analysis of the various thermal ion heating effects for ion traps with a variety of materials including semiconductor electrodes and ion trap control voltage sources that can be easily programmed in a scalable design.

Multi-level and planar ion trap designs are introduced in Section 2. A detailed analytical analysis of the thermal fluctuation ion heating is presented in Section 3 for heating along each of the three principal axes of an ion trap. The results of this analysis are applied to a two-level ion trap representative of what is currently used in quantum computing experiments and a recently proposed scalable multiplexed planar ion trap design. Ion heating associated with noise on the RF voltage drive is discussed in Section 4. Section 5 compares our analytical results with current experiments. And in Section 6, we summarize our results and suggest strategies for minimizing the thermal noise ion heating.

## 2 Ion Trap Designs and Materials

### *2.1 Multi-level Ion Traps*

Present traps typically have two or three levels of electrodes. The ions are trapped in a space between the electrodes. An example of a two-level trap is shown in Fig. 1 [1]. Ion traps with three levels of electrodes are also used in experiments with the control electrodes positioned above and below the RF trapping electrodes [2]. The materials used in present traps are typically gold electrodes and either alumina or silica insulator and support structures. The distances of the trapped ion from the electrodes varies in the range from 100 to 400 $\mu$m.

Ion heating in the traps studied to date appears to arise from sources other than thermal noise, possibly fluctuations in "patch" potentials on the gold electrodes [3]. It is not clear why these patch potentials should be varying at frequencies near the ion vibrational frequencies, in the range between 1 and 10 MHz. There is accumulating evidence that the obseved heating rates vary inversely as the fourth power of the ion/electrode distance [2], instead of the inverse square variation expected from thermal noise heating. Grain boundaries in the gold should vary in size and contact potential at much slower rates. At the UHV pressures in ion traps there are few organic contaminants that could be moving rapidly across the electrode surfaces. Controlled experiments need to be performed in order to understand the heating rates. Temperature, surface roughness, and material composition could be varied along with the distance of the ion from the electrode in order to better understand the anomalous "patch" field heating. The thermal noise heating rates due to the surface resistance of the gold are in the range near 1 $s^{-1}$ (one motional quanta per second) for the present traps, since the

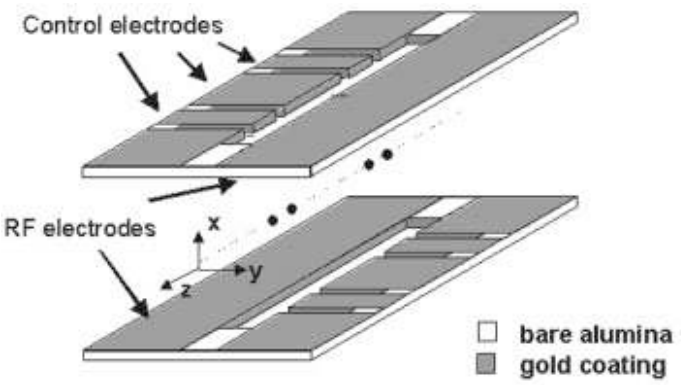


Fig. 1. Present day two-level ion trap. RF potentials are applied to two opposite electrodes for confinement along the $x$- and $y$-axes, and DC potentials are applied to the remaining (control) electrodes for confinement and moving ions along the $z$-axis. Figure courtesy of M.A. Rowe, NIST.

gold has a very low resistivity and the cross-sectional area of the electrodes is relatively large. However, care must be taken to minimize the resistance in the control electrode circuits in order to avoid heating from series resistances.

### *2.2 Planar Ion Traps*

Planar ion traps contain both RF and control electrodes within or near a common plane. The ion is trapped above the plane and can be cooled or excited by laser beams propagating parallel to the surface of the trap. Initial designs of planar traps [4] use gold electrodes on silica or quartz substrates. A number of geometries have been considered. Planar ion traps have been demonstrated experimentally [5] using relatively large electrode and ion/electrode dimensions (of order millimeters) and macroscopic ions. Recently the original planar trap designs [4] have been demonstrated experimentally with Mg ions [6]. These initial experiments are encouraging since the measured ion heating rates are in the same range as those in the more conventional two-level traps.

Planar trap structures can be easily spatially multiplexed [7] to build up an ion trap architecture that can be scaled [8] to large numbers of ions, in the range of thousands of ions/cm$^2$. An example of a scalable ion trap based on silicon VLSI fabrication technology is shown in Fig. 2.

With RF electrode spacing near 100 $\mu$m the ion is trapped at a vertical distance of approximately 50 $\mu$m above the planar surface. This 50 $\mu$m is required in order to propagate the laser beam over the surface of the ion traps without it being distorted or scattered. Note that the ion/electrode spacing in this planar trap example is a factor of 2 to 10 smaller than in the multilevel traps. As a result of the inverse square dependence of thermal noise heating, we expect that ion heating from thermal noise sources will be from 4 to 100 times larger for the planar traps as compared to present day multi-level traps. The RF electrodes are fabricated using metals, e.g. tungsten or gold. The RF electrodes are isolated from the control electrodes by a 10 $\mu$m thick layer of $SiO_2$ that will withstand the large RF voltages required in this type

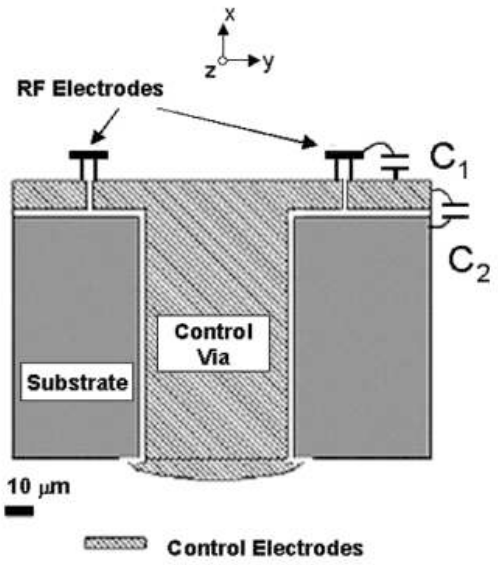


Fig. 2. Scalable ion trap design. The metal RF electrodes are spaced by 100 $\mu$m and are deposited on 10 $\mu$m high $SiO_2$ pedestals. The central control electrode is connected to underlying electronics by a via shown here as a column extending downward. The control electrodes are separated by thin layers of $SiO_2$.

of trap.

The control electrodes can be formed by either a thin layer of metal, or, as shown in Fig. 2, a thick layer of highly doped polysilicon. The doped polysilicon has a resistivity nearly 200 times higher than metals so that a thicker layer is required for a resistance comparable to the metallic case. The control electrodes are electrically isolated from one another by thin thermal oxide layers that extend down through the polysilicon as shown in cross-section in Fig. 2. Silicon fabrication techniques may allow very smooth electrode features, approaching atomic smoothness in some cases. It has been noted that rough surfaces enhance the ion heating mechanisms present in the current traps. Smooth surfaces may become more important as the ion/electrode distance decreases. Materials other than gold may have thin oxide coatings; polysilicon is one example. These oxides can potentially cause ion heating or trap distortion problems that could add to anomalous patch and thermal noise heating.

The RF voltages on the control electrodes are grounded by a capacitive divider network indicated schematically by the capacitances $C_1$ and $C_2$ in Fig. 2. The small capacitance between the RF electrodes and the control electrodes is determined by the 10 $\mu$m thick $SiO_2$ electrode support layer. The much larger capacitance between the control electrodes and the substrate is determined by a thin $SiO_2$ insulating layer and the relatively large area under the control electrodes. The ratio of $C_2/C_1$ is approximately 300, large enough to maintain a low RF level on the control electrode and symmetrize the trap (see Section 4).

The skin depth of the RF trapping fields at frequencies near 100 MHz is large compared to the RF and control electrode thicknesses used in the examples we will analyze. For example, the skin depth for tungsten is 20 $\mu$m and the skin depth for highly doped polysilicon is 200

$\mu$m at an RF frequency of 50 MHz. We will approximate the resistances from the material resistivites and the physical dimensions of the electrodes.

## 3 Ion heating by resistive thermal fluctuations

In this section we consider ion heating by resistive thermal fluctuations using two alternative methods. The first starts with the voltage fluctuations on the trap electrodes caused by thermal noise in the resistance of the electrodes and drive circuits and proceeds to calculate their effect on the ion motion. The second starts with currents induced in the trap electrodes by ion motion and uses the fluctuation-dissipation theorem to relate the power dissipated in the resistive elements to the ion heating rates. The fluctuation-dissipation theorem guarantees the equivalence of these two methods, but for different electrode geometries and sources of resistance it is computationally easier to use one or the other. After describing the methods and applying them to a few simple geometries, we present resistive thermal fluctuation heating rates for both current two-level and proposed planar ion traps.

### *3.1 Direct calculations of the ion heating rate*

For this first method of computing ion heating rates, we start with the spectral density of the voltage fluctuations on the trap electrodes. We relate the spectral density of voltage fluctuations on the trap electrodes to the spectral density of electric field fluctuations at the ion position for several electrode geometries, and we use the spectral density of electric field fluctuations to find the ion heating rate. This method is well established in the literature [9, 3], and it will be referred to as the direct method of computing ion heating rates in this paper.

The spectral density of voltage fluctuations on each trap electrode $S_V(\omega)$ is generated by Johnson noise in the resistance of its drive circuit,

$$S_V(\omega) = 4k_B T R(\omega) \ , \tag{1}$$

where $R(\omega)$ is the real part of the complex impedance $Z(\omega)$ at frequency $\omega$. Voltage fluctuations on the trap electrodes generate electric field fluctuations at the ion position which give rise to heating. The spectral density of voltage fluctuations and the spectral density of electric field fluctuations along the $i$ principal axis ($i \in \{x, y \ or \ z\}$) of the ion motion $S_{E_i}(\omega)$ are related to each other by

$$S_{E_i}(\omega) = \frac{S_V(\omega)}{d_i^2} \ , \tag{2}$$

where the length scale $d_i$ is obtained by solving for the electric field component along the $i$ principal axis at the equilibrium ion position $(x_0, y_0, z_0)$ due to a voltage $V$ on the trap electrode and using

$$E_i(x_0, y_0, z_0) = \frac{V}{d_i} \ . \tag{3}$$

One can then compute the heating rate using time-dependent perturbation theory:

$$\dot{n}_i = \frac{q^2}{4m\hbar\omega_i} S_{E_i}(\omega_i) \ , \tag{4}$$

which gives the average number of harmonic oscillator quanta gained per unit time by the ion motion along the $i$ principal axis [10, 9]. Here $q$ is the ion charge, $m$ is the ion mass, and $\omega_i$ is

the ion secular frequency along the $i$ principal axis. We now compute $d_i$ for several electrode geometries.

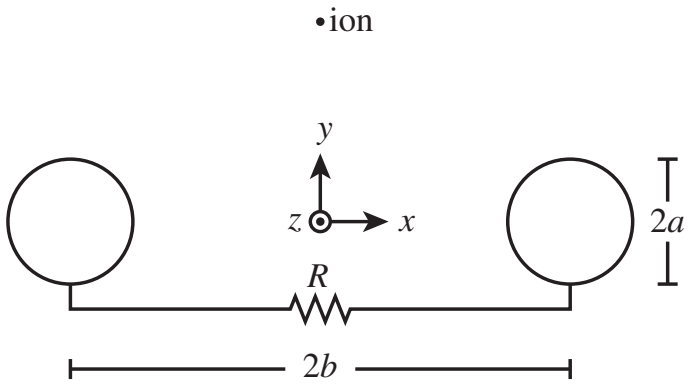


Fig. 3. Geometry for a model of thermal voltage fluctuation ion heating by the resistance between two parallel trap electrodes. The two circular electrodes extend indefinitely in the $z$ direction. Voltage fluctuations in the resistor generate electric field fluctuations in the $x$ direction at the ion position $(0, y, 0)$, which heat the ion motion.

The first geometry models ion heating due to the thermal voltage fluctuations in a resistor between two parallel circular cylinders of radius $a$ and infinite length (see Fig. 3). This could be a model of heating of the $x$ motion in a planar ion trap due to the finite resistivity of the RF electrode material or a model of the $x$ and $y$ heating in a two-level trap where the resistance is primarily that in the filter networks used to suppress capacitive pickup of the RF drive on the control electrodes. Electrodes besides the two in question are ignored in this model. The coordinate system is constructed such that the electrodes are parallel to the $z$-axis. The two electrodes are located at $(x, y) = (\pm b, 0)$ and are biased at $\mp V/2$, respectively. As can be verified by checking that it satisfies both Laplace's equation and the boundary conditions, the potential outside the electrodes is given by

$$\phi(x,y) = \frac{V}{2\cosh^{-1}(b/a)} \ln \sqrt{\frac{(x-\sqrt{b^2-a^2})^2+y^2}{(x+\sqrt{b^2-a^2})^2+y^2}} \; . \tag{5}$$

The charge on a segment of length $l$ of one of the electrodes

$$Q = \mp \frac{\pi\epsilon_0 V}{\cosh^{-1}(b/a)} l \; , \tag{6}$$

and thus the capacitance between the two electrodes is given by

$$C = \frac{\pi\epsilon_0}{\cosh^{-1}(b/a)} l \; . \tag{7}$$

In the cases we consider this capacitance is not large enough to suppress the voltage fluctuations on the trap electrodes. The electric field at the ion position,

$$\mathbf{E}(0,y,0) = \frac{V}{\cosh^{-1}(b/a)} \frac{\sqrt{b^2-a^2}}{y^2+b^2-a^2} \hat{\mathbf{i}} \; , \tag{8}$$

is in the $x$ direction and hence thermal voltage fluctuations in the resistance between the two electrodes heat the $x$ mode of the ion motion. The length scale is given by

$$d_x = \cosh^{-1}(b/a)\frac{y^2 + b^2 - a^2}{\sqrt{b^2 - a^2}} \tag{9}$$

for this geometry.

For other geometries we compute the length scales $d_i$ numerically. We solve for the electric field at the ion position using a finite element electrostatics solver. The electrode of interest is biased at a potential $V$ and the other electrodes are held at ground. Because the monopole term of this charge distribution can be nonzero care must be taken to implement the boundary condition $\lim_{|\mathbf{r}|\to\infty} \phi(\mathbf{r}) = 0$ properly, particularly for the open geometries of planar ion traps. We then use Eq. 3 to compute the length scales $d_i$. Results are presented in Sections 3.3 and 3.4 where detailed specifications of trap geometries are given.

### *3.2 Indirect calculations of the ion heating rate*

The second method of calculating rates for ion heating by resistive thermal fluctuations relies on a fundamental link, between these fluctuations and energy dissipation, established by the fluctuation dissipation theorem. Energy is dissipated when an ion moves within an ion trap. This energy is dissipated as the currents, that redistribute the charge on the electrodes as the ion moves, flow through the resistive electrode material or through the resistance of the drive circuits. As a consequence, an ion experiences damped motion characterized by a friction coefficient. According to the fluctuation-dissipation theorem, this friction coefficient and the trap circuitry temperature uniquely determine the spectral density of the electric field fluctuations at the ion. Hence, determining the spectral density is reduced to the problem of calculating a friction coefficient that can often be obtained by a simple classical analysis. As long as the ion/resistive-element coupling is linear (as is the case for a charge coupled electrostatically to a linearly resistive object) the value of this coefficient is the same regardless of whether one does a fully quantum calculation or a fully classical calculation. The damping coefficient does not depend on the state of the system, in particular on the ion state. The ion state can be described by a quantum state (e.g. a Fock or coherent state) without changing the validity of this calculation. We note that in particular this indirect method can handle heating due to nonzero electrode resistivity much more easily than the direct method.

The power dissipated by currents induced in the trap electrodes by an ion whose position along the $x$ principal axis is given by $x = x_m \sin(\omega_x t)$ can be calculated for a given electrode geometry by solving for the charge induced in the trap electrodes as a function of time. The dissipated power can be described in terms of a friction coefficient for the ion motion $\mu$ defined by

$$F_x = -\mu\frac{dx}{dt} \ . \tag{10}$$

In terms of $\mu$, the power dissipated is given by

$$P = \mu\left\langle\left(\frac{dx}{dt}\right)^2\right\rangle = \frac{\mu x_m^2 \omega_x^2}{2} \ , \tag{11}$$

which can be equated to the power dissipated in the trap electrodes to yield an expression for the friction coefficient. The brackets denote time averaging. The fluctuation-dissipation

theorem relates the friction coefficient defined by Eq. 10 to the spectral density of the force fluctuations (in the high electrode temperature limit),

$$S_{F_x}(\omega) = 4k_B T\mu \ , \tag{12}$$

for general linear dissipative systems [11]. The spectral density of electric field fluctuations, obtained by dividing Eq. 12 by $q^2$, is then used to compute the ion heating rate via Eq. 4. We now compute the dissipated power for two electrode geometries.

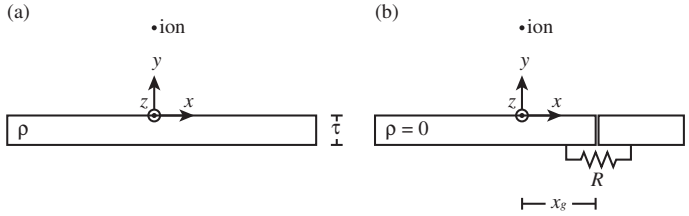


Fig. 4. Geometries for two models of resistive thermal fluctuation ion heating by planar electrodes. The electrodes extend indefinitely in the $x$ and $z$ directions. (a) Here ion motion along any of the principal axes induces currents in the resistive planar electrode below it. The fluctuations concomitant to this dissipation heat all three modes of the ion motion. (b) In this model, ion motion along either of the $x$ or $y$ principal axes induces a current in the resistor between two perfectly conducting semi-infinite planar electrodes.

First consider the power dissipated by a slab of material of resistivity $\rho$ depicted in Fig. 4(a). This is a model of the control electrodes in a planar ion trap. The electric field of an ion located at $(x, y, z) = (x_m \sin(\omega_x t), y_0, 0)$ above a perfectly conducting infinite slab of material whose top surface is located at $y = 0$ is found by the method of images to be

$$\begin{aligned} \mathbf{E}(x,y,z) &= \frac{q[(x - x_m\sin(\omega_x t))\mathbf{i} + (y - y_0)\mathbf{j} + z\mathbf{k}]}{4\pi\epsilon_0[(x - x_m\sin(\omega_x t))^2 + (y - y_0)^2 + z^2]^{3/2}} \\ &- \frac{q[(x - x_m\sin(\omega_x t))\mathbf{i} + (y + y_0)\mathbf{j} + z\mathbf{k}]}{4\pi\epsilon_0[(x - x_m\sin(\omega_x t))^2 + (y + y_0)^2 + z^2]^{3/2}} \ . \end{aligned} \tag{13}$$

The surface charge density $\rho_s = \epsilon_0 \mathbf{E} \cdot \mathbf{j}$ is thus given by

$$\rho_s(x,z) = -\frac{qy_0}{2\pi((x - x_m\sin(\omega_x t))^2 + y_0^2 + z^2)^{3/2}} \ . \tag{14}$$

The surface current density can be obtained using charge conservation in two dimensions,

$$\frac{\partial \rho_s}{\partial t} + \nabla \cdot \mathbf{J}_s = 0 \ , \tag{15}$$

and the boundary condition $\lim_{|\mathbf{r}|\to\infty} \mathbf{J}_s(\mathbf{r}) = 0$:

$$\mathbf{J}_s(x,z) = -\frac{qx_m y_0 \omega_x \cos(\omega_x t)\mathbf{i}}{2\pi[(x - x_m\sin(\omega_x t))^2 + y_0^2 + z^2]^{3/2}} \ . \tag{16}$$

Now consider that the slab is not perfectly conductive but has resistivity $\rho$ and thickness $\tau$. For skin depth

$$\delta(\omega_x) = \sqrt{\frac{2\epsilon_0 c^2 \rho}{\omega_x}} \gg \tau \tag{17}$$

the surface current density $\mathbf{J}_s$ will be uniformly distributed through the thickness of the slab, such that the volume current density is given by

$$\mathbf{J}(x,y,z) = -\frac{qx_m y_0 \omega_x \cos(\omega_x t)\mathbf{i}}{2\pi\tau[(x - x_m \sin\omega_x t)^2 + y_0^2 + z^2]^{3/2}} \tag{18}$$

for $-\tau < y < 0$. Eq. 17 is satisfied for all of the electrodes which we consider; for example the skin depth of tungsten at 10 MHz is 36 $\mu$m whereas proposed planar ion trap designs use tungsten electrodes with thickness around 0.25 $\mu$m. The dissipated power for this geometry is given by

$$P = \int_{-\infty}^{\infty} \mathrm{d}x \int_{-\tau}^{0} \mathrm{d}y \int_{-\infty}^{\infty} \mathrm{d}z \rho \langle |\mathbf{J}(x,y,z)|^2 \rangle = \frac{\rho q^2 x_m^2 \omega_x^2}{16\pi\tau y_0^2} \tag{19}$$

where the angle brackets denote time averaging. The spectral density of electric field fluctuations parallel to a resistive plane is thus

$$S_{E_i}(\omega) = \frac{k_B T \rho}{2\pi y_0^2 \tau} \ . \tag{20}$$

A similar analysis considering ion motion in the $y$ direction shows that the spectral density of electric field fluctuations perpendicular to a resistive plane is identical, thus the above equation holds for all $i$. If we replace $\tau$ with $\delta(\omega)$ in Eq. 20 it shows the same scaling as the limit $\delta(\omega) \ll y_0$ of the results reported in [12] and [3], which are derived for $\delta(\omega) \ll \tau$.

The second geometry we consider is again a planar electrode. This time, however, the electrode is segmented perpendicular to the ion motion as shown in Fig. 4(b) and we consider dissipation in the resistance between the two half-planes. This is a model of dissipation in the drive circuits of adjacent control electrodes in a planar ion trap. Again let the ion be located at $(x,y,z) = (x_m \sin(\omega_x t), y_0, 0)$ and the upper surface of the electrodes be located at $y = 0$. The two electrodes are electrically isolated by an infinitesimal gap at $x = x_g$ and connected through a resistance $R$. The charges on the electrodes $x < x_g$ and $x > x_g$ are

$$Q_< = \int_{-\infty}^{x_g} \mathrm{d}x \int_{-\infty}^{\infty} \mathrm{d}z \rho_s(x,z) = -\frac{q}{2} - \frac{q}{\pi} \tan^{-1}\left[\frac{x_g}{y_0} + \frac{x_m}{y_0}\sin(\omega_x t)\right] \tag{21}$$

and

$$Q_> = -q - Q_< \tag{22}$$

where $\rho_s$ is given by Eq. 14. The power dissipated by the current flowing between the two electrodes is given by

$$P = \left\langle (dQ_</dt)^2 \right\rangle R = \frac{Rq^2 x_m^2 \omega_x^2}{2\pi^2 y_0^2} \left[ \frac{1}{\left(1 + \left(\frac{x_g}{y_0}\right)^2\right)^2} + \mathcal{O}\left(\frac{x_m}{y_0}\right)^2 \right] \ . \tag{23}$$

Since $x_m$ is of the order of the size of the ion's ground state wavefunction, $x_m/y_0$ is very small and we drop the second order correction. The spectral density of electric field fluctuations in the $x$ direction is thus given by

$$S_{E_x}(\omega) = \frac{4k_B T R}{\pi^2 y_0^2} \frac{1}{\left(1 + \left(\frac{x_g}{y_0}\right)^2\right)^2} \ . \tag{24}$$

Table 1. Two-level ion trap parameters

| Parameter | Value |
|---|---|
| Gap width, $w_g$ | 400 $\mu$m |
| Gap height, $h_g$ | 360 $\mu$m |
| Electrode width, $w_e$ | 1 mm |
| Electrode height, $h_e$ | 200 $\mu$m |
| RF electrode length, $l_{RF}$ | 4 mm |
| Endcap control electrode length scale, $V_c/E_z(x_0, y_0, z_0)$ | 4.1 mm |
| Electrode sheet resistance, $\rho/h_e$ | 5.7 m$\Omega/\Box$ (m$\Omega$ per square) |
| Control electrode filter network resistor, $R_c$ | 1 k$\Omega$ |
| Control electrode filter network capacitor, $C_c$ | 820 pF |
| Electrode temperature, $T$ | 300 K |
| RF drive frequency, $\Omega$ | $2\pi \times 230$ MHz |
| Radial secular frequency, $\omega_x = \omega_y$ | $2\pi \times 6$ MHz |
| Axial secular frequency, $\omega_z$ | $2\pi \times 2.9$ MHz |

Upon similar analyses we find that the spectral density of electric field fluctuations in the $y$ direction is given by

$$S_{E_y}(\omega) = \frac{4k_BTR}{\pi^2 y_0^2} \frac{\left(\frac{x_g}{y_0}\right)^2}{\left(1 + \left(\frac{x_g}{y_0}\right)^2\right)^2}, \tag{25}$$

and there are no electric field fluctuations in the $z$ direction for this geometry.

### *3.3 Ion heating rates for two-level traps*

In this section we present rough estimates of the resistive thermal fluctuation heating rates in a two-level ion trap representative of what is currently used in quantum computation experiments. Current multi-level ion traps are typically made by depositing 0.3 – 3.5 $\mu$m thick gold electrodes on alumina wafers [3, 1, 2]. We present heating rates for the two-level trap geometry used in [1] and shown in Fig. 5; the relevant parameters are summarized in Tab. 1.

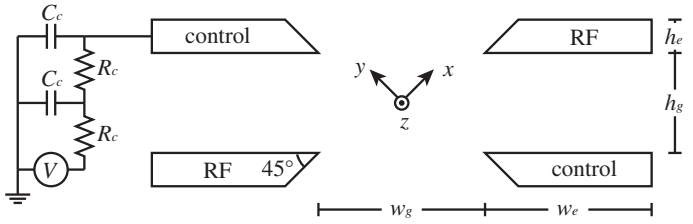


Fig. 5. Schematic showing two-level ion trap geometry and control electrode filter network. The RF and control electrodes are labeled, and the principal axis coordinate system is drawn at the ion location. The trap is translationally invariant along the $z$ axis except that the control electrodes are segmented to provide axial confinement.

Thermal heating in current two-level traps is dominated by the resistors in the filter networks used to suppress capacitive pickup of the RF drive voltage on the control electrodes.

Table 2. Two-level ion trap heating rates for $^9$Be

| Mechanism | $S_{E_i}(\omega_i)$ $[(\mathrm{V/m})^2\ \mathrm{Hz}^{-1}]$ | $\dot{n}_i$ $[\mathrm{s}^{-1}]$ |
|---|---|---|
| $x$ heating by resistance of control electrode filter network | 0 | 0 |
| $x$ heating by resistance between RF electrodes | $1.4 \times 10^{-16}$ | $1.5 \times 10^{-2}$ |
| $x$ heating by resistivity of electrode material | $2.4 \times 10^{-17}$ | $2.5 \times 10^{-3}$ |
| Total $x$ resistive thermal fluctuation heating | $1.6 \times 10^{-16}$ | $1.7 \times 10^{-2}$ |
| $y$ heating by resistance of control electrode filter network | $1.7 \times 10^{-14}$ | 1.8 |
| $y$ heating by resistance between RF electrodes | 0 | 0 |
| $y$ heating by resistivity of electrode material | $2.4 \times 10^{-17}$ | $2.5 \times 10^{-3}$ |
| Total $y$ resistive thermal fluctuation heating | $1.7 \times 10^{-14}$ | 1.8 |
| $z$ heating by resistance of control electrode filter network | $4.2 \times 10^{-15}$ | 0.95 |
| $z$ heating by resistivity of electrode material | $2.4 \times 10^{-17}$ | $5.2 \times 10^{-3}$ |
| Total $z$ resistive thermal fluctuation heating | $1.7 \times 10^{-14}$ | 3.8 |

Here the filter networks are composed of two cascaded RC low pass filters with effective resistance

$$R(\omega) = \mathrm{Re}[Z(\omega)] = \frac{2 + (\omega R_c C_c)^2}{1 + 7(\omega R_c C_c)^2 + (\omega R_c C_c)^4} \ . \tag{26}$$

Heating along the $z$ principal axis by this resistance is computed using the direct method with the scale length computed by [1] and repeated in Tab. 1. Heating rates along the $x$ and $y$ principal axes by this resistance are computed using the model of two parallel circular cylinders with separation $2b = \sqrt{(w_g + h_e)^2 + (h_g + h_e)^2}$, radius $a = h_e/2$, and resistance $R = (2/3)R(\omega_i)$. The latter is reasonable because three control electrodes (three filter networks hooked up in parallel) correspond to each of the two cylinders (which are effectively connected in series). The ion is located at $y = 0$.

The $x$ and $y$ heating by the resistance between the RF electrodes is likewise computed using the direct method with the electric field fluctuations modeled by two parallel circular cylinders. This time the resistance is due to the resistivity of the electrode material and is estimated as $R = l_{RF}\rho/(4w_e h_e)$, which is a reasonable approximation when the RF electrodes are electrically connected at both ends.

The heating due to the resistivity of the electrode material is estimated using the indirect method for heating above a resistive plane: Eq. 20 with $y_0 = w_g/2$. While this model provides only a zeroth order estimate of the heating rate for this two-level electrode geometry, the results show that heating by the resistivity of the electrode material is orders of magnitude smaller than heating by the resistance of the control electrode filter networks so we do not pursue a more accurate model.

Resistive thermal fluctuation heating rates for the ion trap parameters given in Tab. 1 are presented in Tab. 2. The $z$ heating due to the resistance of the control electode filter network is given per control electrode in Tab. 2. There are two control electrode sets consisting of three control electrode segments each, for a total of six control electrodes. An ion in the center of the trap that oscillates in the z direction induces currents in four of these control electrodes, i.e. the two end electrodes in each set. Thus the total z heating rate includes four times the heating rate due to one control electrode filter network. The total heating rate along the $z$ axis is a few motional quanta per second, which corresponds to a decoherence time for the

ion's motional state of a few hundred milliseconds. This is the principal axis of most interest to the quantum computing community, as the motional state along this axis is used as the data bus for two qubit gates. The total heating rates along the other principal axes are of the same order of magnitude. The heating rates which are measured experimentally in current ion traps are two orders of magnitude larger, so ion heating by resistive thermal fluctuations is considered unimportant [3] in the relatively large traps in present use.

### *3.4 Ion heating rates for planar traps*

This section presents some estimates of the resistive thermal fluctuation heating rates for the planar ion traps described in Section 2.2. Fig. 6 shows the particular geometry we consider, and Tab. 3 gives the dimensions and impedances expected of first generation planar traps. Resistive thermal fluctuation heating is caused by the resistance of the control electrode voltage source as well as the resistivities of the RF and control electrode materials. The control electrode voltage source is again the largest source of thermal heating, but the material resistivities are no longer negligible.

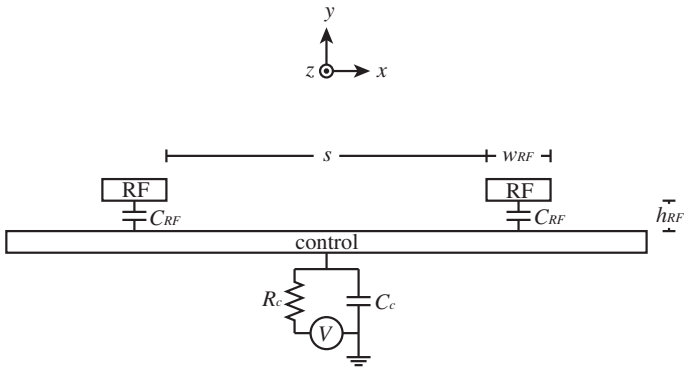


Fig. 6. Schematic showing planar ion trap geometry. The ion is located at $(x, y, z) = (x_0, y_0, z_0)$ and the principal axes of the ion motion are oriented as shown. The RF and control electrodes extend $l_{RF}$ in the $z$ direction, with the control electrode segmented to provide axial confinement. $h_{RFe}$ is the RF electrode thickness and $h_{ce}$ is the control electrode thickness. Both of these thicknesses are typically near $1\mu m$.

The resistance of the control electrode voltage source is a combination of the resistances of the thru-wafer via which connects the ion trap chip to the integrated control chip, the CMOS multiplexers used to distribute a few signals to many control electrodes, and the associated semiconductor wiring. The shunt capacitance between the control electrodes and ground is not expected to be large enough to mitigate the resistive thermal fluctuations. If the control electrodes are split along either $x = 0$ or $x = \pm(s + w_{RF})/2$ in order to allow control voltages to tilt the principal axes for laser cooling, the $x$ ion motion will be heated by the control electrode voltage source resistance. The heating rates for both cases are computed using Eq. 24 with $R = 2R_c$. We compute the $z$ heating rates using the same equation for control electrode segments with various positions relative to the ion. The $z$ heating rate is very large when an ion is directly over a gap between the electrode segments, but this only happens for a short time when ions are being moved between trap regions. Finally, the $y$ heating rates due to the voltage source resistance for control electrodes segmented both parallel and

Table 3. Planar ion trap parameters

| Parameter | Value |
|---|---|
| RF electrode separation, $s$ | 100 $\mu$m |
| RF electrode width, $w_{RF}$ | 20 $\mu$m |
| RF electrode length, $l_{RF}$ | 1 mm |
| Height of RF electrode support, $h_{RF}$ | 10 $\mu$m |
| Location of electric quadrupole null (ion location), $(x_0, y_0, z_0)$ | (0, 59 $\mu$m, 0) |
| Control electrode length scale, $V_c/E_y(x_0, y_0, z_0)$ | 840 $\mu$m |
| RF electrode sheet resistance, $\rho_{RF}/h_{RFe}$ | 0.2 $\Omega/\square$[a] |
| Control electrode sheet resistance, $\rho_c/h_{ce}$ | 0.2 $\Omega/\square$[b] |
| Control electrode source resistance (via, MUX, and wiring), $R_c$ | 30 $\Omega$ |
| Electrode temperature, $T$ | 300 K |
| RF drive frequency, $\Omega$ | $2\pi \times 100$ MHz |
| Radial secular frequency, $\omega_x = \omega_y$ | $2\pi \times 10$ MHz |
| Axial secular frequency, $\omega_z$ | $2\pi \times 5$ MHz |

[a]This is appropriate for 0.25 $\mu$m of tungsten.
[b]This is appropriate for either 20 $\mu$m of polysilicon or 0.25 $\mu$m of tungsten.

perpendicular to the RF electrodes are computed using Eq. 25.

The resistivity of the RF electrode material primarily heats the $x$ mode of the ion motion. This heating can be significant in a large multiplexed trap because the RF rails on either side of an ion might not be electrically connected nearby. The resistance between the two RF electrodes for a linear trap of length $l_{RF}$ and RF electrode width $w_{RF}$ in which the RF electrodes are electrically connected at both ends is a maximum at the center of the trap and given by $R = (l_{RF}\rho_{RF})/(2w_{RF}h_{RFe})$. We use the direct method with the model of the potential between two parallel circular cylinders to compute the heating rate. The electrode separation $2b$ is taken to be $(s + w_{RF})/2$, the electrode radius $a = w_{RF}/4$, and the ion position $y = y_0 - h_{RF}$. We calculate the heating rate for the $y$ motion due to the RF electrode resistance using the direct method with the control electrode length scale computed numerically in two dimensions and provided in Tab. 4, and the resistance of one RF electrode at the center of a linear trap segment: $R = (l_{RF}\rho_{RF})/(4w_{RF}h_{RFe})$.

The resistivity of the control electrode material heats the ion motion along the $x$, $y$, and $z$ principal axes. The heating rates are computed using the indirect method with Eq. 20. It is seen in Tab. 4 that the heating due to the resistivity of the control electrode material is small.

The analysis here suggests that the resistance of the control electrode voltage source is the largest source of resistive thermal fluctuation heating and will continue to be such for the $z$ motion until $R_c \lesssim 1\ \Omega$. In contrast to current two-level traps, however, heating by the resistivity of the RF electrode material and to a lesser extent the control electrode material is also important and should not be neglected. Note that the heating rates in both Tabs. 2 and 4 are only estimates because of the approximate geometry models we have considered. We think our rate estimates should model actual traps to an accuracy within 50%. For a more accurate analysis of resistive thermal fluctuation heating the approximate geometry models considered here should be replaced by the actual three-dimensional ion trap geometry and the heating rates along each principal axis due to each electrode should be computed numerically.

Table 4. Planar ion trap heating rates for $^9$Be

| Mechanism | $S_{E_i}(\omega_i)$ $[(\mathrm{V/m})^2\ \mathrm{Hz}^{-1}]$ | $\dot{n}_i$ $[\mathrm{s}^{-1}]$ |
|---|---|---|
| $x$ heating by resistance of split control electrode voltage source | | |
| – Split in between RF electrodes | $9.6 \times 10^{-12}$ | 620 |
| – Split under RF electrodes | $1.7 \times 10^{-12}$ | 110 |
| $x$ heating by resistance of RF electrodes | $8.2 \times 10^{-13}$ | 53 |
| $x$ heating by resistivity of control electrode material | $3.8 \times 10^{-14}$ | 2.4 |
| Total $x$ resistive thermal fluctuation heating[a] | $2.5 \times 10^{-12}$ | 160 |
| $y$ heating by resistance of split control electrode voltage source | | |
| – Split in between RF electrodes | 0 | 0 |
| – Split under RF electrodes | $4.7 \times 10^{-12}$ | 300 |
| $y$ heating by resistance of control electrode voltage source | | |
| – Ion directly above gap | 0 | 0 |
| – Ion 50 $\mu$m to side of gap | $2.3 \times 10^{-12}$ | 150 |
| – Ion 100 $\mu$m to side of gap | $1.8 \times 10^{-12}$ | 120 |
| $y$ heating by resistance of RF electrodes | $5.9 \times 10^{-14}$ | 3.8 |
| $y$ heating by resistivity of control electrode material | $3.8 \times 10^{-14}$ | 2.4 |
| Total $y$ resistive thermal fluctuation heating[b] | $3.8 \times 10^{-12}$ | 240 |
| $z$ heating by resistance of control electrode voltage source | | |
| – Ion directly above gap | $9.6 \times 10^{-12}$ | 1200 |
| – Ion 50 $\mu$m to side of gap | $3.3 \times 10^{-12}$ | 420 |
| – Ion 100 $\mu$m to side of gap | $6.4 \times 10^{-13}$ | 83 |
| $z$ heating by resistivity of control electrode material | $3.8 \times 10^{-14}$ | 4.9 |
| Total $z$ resistive thermal fluctuation heating[c] | $6.9 \times 10^{-13}$ | 88 |

[a] Assuming that the control electrodes are split under the RF electrodes.

[b] Assuming that the control electrodes are not split parallel to the RF electrodes for laser cooling and the ion is located over the center of a 200 $\mu$m long control electrode in the $z$ direction with no other control electrode segments nearby. Note that while this is not consistent with the total heating rate presented for the $x$ motion, a more complete analysis would require considering the effect of each two-dimensional control electrode individually.

[c] Assuming that the ion is located over the center of a 200 $\mu$m long control electrode and there are no other control electrode gaps nearby.

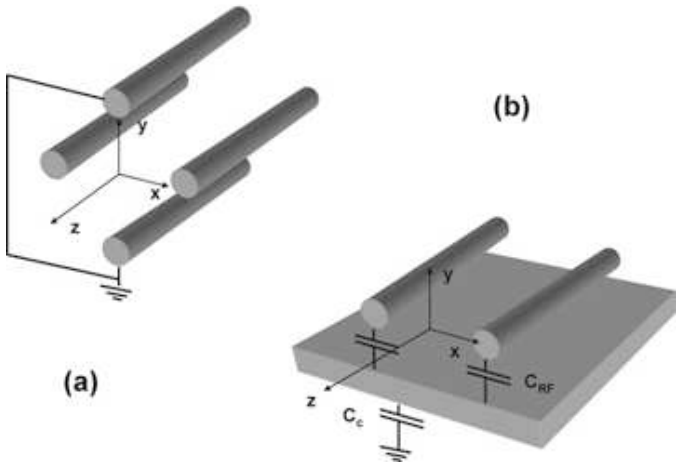


Fig. 7. Schematic drawing of (a) a four rod Paul trap and (b) a planar trap.

## 4 RF Drive Fluctuation Ion Heating

Typically there is considerable noise on the trap electrodes generated by the RF drive. The electrode voltages are generated by an RF resonator, e.g. a helical resonator [13, 14]. The resonator is driven by an RF amplifier with a gain of over 1000. If the noise at the input to this amplifer were near the thermal level for an input resistance of 50 Ω, then the output noise would be quite large. Since the trapping mechanism is a nonlinear process, noise at the sidebands $\Omega \pm \omega_i, \Omega \pm 2\omega_i, \ldots$ of the drive frequency Ω will parametrically mix with and heat the ion motion. In the following we show that while for symmetric traps the noise is common mode and does not heat the ions, RF drive fluctuations do heat the ion motion in asymmetric ion traps. We find that the heating associated with trap asymmetry is negligible for our model planar traps when compared to that caused by thermal fluctuations in the electrodes.

### *4.1 Symmetric Trap Electrodes*

Consider a symmetric Paul trap which confines in the $x - y$ plane but is translationally invariant along the $z$ direction as shown in Fig. 7(a). The trap potential can be written as

$$\phi(x, y) = \frac{1}{2}\left(1 + \frac{x^2 - y^2}{R'^2}\right) V_0 \cos(\Omega t) \tag{27}$$

where Ω is the oscillation frequency of the RF drive and $R'$ is the trap radius of curvature, typically of the order of the electrode separation. The electric field near the ion is then

$$\mathbf{E}(x, y) = -\boldsymbol{\nabla}\phi = -\left(\frac{x\mathbf{i} - y\mathbf{j}}{R'^2}\right) V_0 \cos(\Omega t) \ . \tag{28}$$

The equation of motion for the ion in the $y$ direction is given by

$$m\frac{d^2y}{dt^2} - \frac{qV_0}{R'^2} y \cos(\Omega t) = 0 \ . \tag{29}$$

A similar equation of motion holds in the $x$ direction.

We now make the assumption that the $y$ motion can be separated into a fast part $y_1$ that oscillates at the trap frequency $\Omega \sim 100$ MHz and a slow part $y_0$ that oscillates at a much lower frequency, the secular frequency of the ion $\omega_y \sim 1$ MHz. Then the equation for the motion along the $y$ direction can be decomposed into

$$m\frac{d^2y_0}{dt^2} - \frac{qV_0}{R'^2}y_1\cos(\Omega t) = 0 \tag{30}$$

and

$$m\frac{d^2y_1}{dt^2} - \frac{qV_0}{R'^2}y_0\cos(\Omega t) = 0\ . \tag{31}$$

The fast equation (Eq. 31) can be integrated under the approximation that $y_0$ is constant over one cycle of $y_1$ to yield

$$y_1 = -\frac{qV_0}{m\Omega^2 R'^2}y_0\cos(\Omega t)\ . \tag{32}$$

Substituting this into the slow equation (Eq. 30) yields

$$m\frac{d^2y_0}{dt^2} + \frac{q^2V_0^2}{m\Omega^2 R'^4}y_0\cos^2(\Omega t) = 0 \tag{33}$$

for the secular motion $y_0$. Time averaging $\cos^2(\Omega t)$ we obtain

$$\frac{d^2y_0}{dt^2} + \omega_y^2 y_0 = 0 \tag{34}$$

where the frequency of the ion's secular motion is given by

$$\omega_y = \frac{qV_0}{\sqrt{2}m\Omega R'^2}\ . \tag{35}$$

This analysis is exact in the limit $\Omega \gg \omega_y$.

Proceeding from this well known formulation of ion motion, we add noise to the potential of the RF electrodes which comes from the RF drive electronics. Specifically we consider the case when

$$\phi(x,y) = \frac{1}{2}\left(1 + \frac{x^2-y^2}{R'^2}\right)[V_0\cos(\Omega t) + v_0(t)] \tag{36}$$

where $v_0(t)$ is a fluctuating potential. The equation of motion is now

$$m\frac{d^2y}{dt^2} - \frac{qV_0}{R'^2}\left(\cos(\Omega t) + \frac{v_0(t)}{V_0}\right)y = 0\ . \tag{37}$$

We again separate $y$ into slow and fast parts $y_0$ and $y_1$, governed by

$$m\frac{d^2y_0}{dt^2} - \frac{qV_0}{R'^2}\left(\cos(\Omega t) + \frac{v_0(t)}{V_0}\right)y_1 = 0 \tag{38}$$

and

$$m\frac{d^2y_1}{dt^2} - \frac{qV_0}{R'^2}\left(\cos(\Omega t) + \frac{v_0(t)}{V_0}\right)y_0 = 0\ . \tag{39}$$

Integrating the latter equation we obtain

$$y_1 = -\frac{qV_0}{m\Omega^2 R'^2}\left(\cos(\Omega t) - \Omega^2 \int \mathrm{d}t \int \mathrm{d}t \frac{v_0(t)}{V_0}\right) y_0 \ . \tag{40}$$

Substituting this into the prior equation and time averaging $\cos^2(\Omega t)$ yields

$$\frac{d^2 y_0}{dt^2} + \omega_y^2 \left[1 + 2\frac{v_0(t)}{V_0}\cos(\Omega t) - 2\cos(\Omega t)\Omega^2 \int \mathrm{d}t \int \mathrm{d}t \frac{v_0(t)}{V_0}\right] y_0 = 0 \tag{41}$$

where we have dropped the term second order in $v_0(t)/V_0$. The first order fluctuation terms $v_0(t)/V_0$ act as a fluctuating correction to the secular frequency and give rise to ion motion phase noise. We thus see that to first order, fluctuations on the trap potential do not give rise to heating in a symmetric trap (though they do give rise to phase decoherence).

### *4.2 Asymmetric trap electrode geometries*

The planar ion trap is actually rather asymmetric as seen in Fig. 7(b). The electrodes at RF ground are the control electrode (shown as a plate in Fig. 7(b)) and a distant ground (typically the vacuum chamber). The potential near the ion position can be written as

$$\phi(x,y) = \frac{1}{2}\left(1 + \frac{x^2 - y^2}{R'^2} + \frac{2\alpha y}{R''}\right)\left[V_0 \cos(\Omega t) + v_0(t)\right] \ . \tag{42}$$

where $R''$ is a geometry dependent scale length that sets the electric potential slope at the ion trapping site. Because the control electrode is capacitively coupled to the RF electrodes, there is an extra term in the potential which is linear in $y$ and proportional to the voltage on the RF electrodes. The constant of proportionality is given by the capacitive voltage divider consisting of the capacitances between the RF electrodes and the control electrode $C_{RF}$ and the capacitance between the control electrode and ground $C_c$:

$$\alpha = \frac{V_c}{V_{RF}} = \frac{2C_{RF}}{2C_{RF} + C_c} \ . \tag{43}$$

Writing the equation of motion in the $y$ direction and separating it into fast and slow parts as before, we obtain

$$m\frac{d^2 y_0}{dt^2} - \frac{qV_0}{R'^2}\left(\cos(\Omega t) + \frac{v_0(t)}{V_0}\right)\left(y_1 - \alpha\frac{R'^2}{R''}\right) = 0 \tag{44}$$

and

$$m\frac{d^2 y_1}{dt^2} - \frac{qV_0}{R'^2}\left(\cos(\Omega t) + \frac{v_0(t)}{V_0}\right)\left(y_0 - \alpha\frac{R'^2}{R''}\right) = 0 \ . \tag{45}$$

Solving Eq. 45 for the fast motion

$$y_1 = -\frac{qV_0}{m\Omega^2 R'^2}\left(\cos(\Omega t) - \Omega^2 \int \mathrm{d}t \int \mathrm{d}t \frac{v_0(t)}{V_0}\right)\left(y_0 - \alpha\frac{R'^2}{R''}\right) \tag{46}$$

and substituting the result into Eq. 44 gives

$$\begin{aligned} \frac{d^2 y_0}{dt^2} \quad &+ \quad \omega_y^2 \left[2\cos^2(\Omega t) + 2\frac{v_0(t)}{V_0}\cos(\Omega t) - 2\cos(\Omega t)\Omega^2 \int \mathrm{d}t \int \mathrm{d}t \frac{v_0(t)}{V_0}\right]\left(y_0 - \alpha\frac{R'^2}{R''}\right) \\ &+ \quad \sqrt{2}\alpha\Omega\omega_y \frac{R'^2}{R''}\left(\cos(\Omega t) + \frac{v_0(t)}{V_0}\right) = 0 \ . \end{aligned} \tag{47}$$

Since the components of $v_0(t)$ which will give rise to the largest heating are at $\Omega \pm \omega_y$, we can approximate the double integral as $-v_0(t)/\Omega^2$. Averaging $\cos^2(\Omega t)$ and dropping the terms which do not have a component at $\omega_y$, we obtain

$$\frac{d^2y_0}{dt^2} + \omega_y^2 \left[1 + 4\frac{v_0(t)}{V_0}\cos(\Omega t)\right] y_0 - 2\sqrt{2}\alpha\frac{\omega_y}{\Omega}\frac{q}{m}\frac{v_0(t)\cos(\Omega t)}{R''} = 0 \ . \tag{48}$$

Of the remaining terms, the last one has a component at $\omega_y$ due to the components of $v_0(t)$ at $\Omega \pm \omega_y$ which gives rise to ion heating independent of $y_0$. Using the formalism of [15], this can be written as

$$\frac{d^2y_0}{dt^2} + \gamma\frac{dy_0}{dt} + \omega_y^2 \left[1 + 4\frac{v_0(t)}{V_0}\cos(\Omega t)\right] y_0 = 2\gamma\frac{dy_0^{in}}{dt} \ , \tag{49}$$

with incoming fluctuations given by

$$2\gamma\frac{dy_0^{in}}{dt} = 2\sqrt{2}\alpha\frac{\omega_y}{\Omega}\frac{q}{m}\frac{v_0(t)\cos(\Omega t)}{R''} \tag{50}$$

and the associated dissipation term

$$\gamma\frac{dy_0}{dt} \tag{51}$$

written in by hand. Hence the spectral density of electric field fluctuations which goes into Eq. 4 to compute the heating rate is

$$\frac{\alpha^2}{2}\frac{\omega_y^2}{\Omega^2}\frac{S_V(\Omega \pm \omega_y)}{R''^2} \tag{52}$$

For the planar ion trap geometry described in Section 3.4, $\alpha = 4 \times 10^{-3}$ and $R'' = 840\ \mu$m. The value used here for $R''$ is obtained from a numerical calculation of the planar trap potential. If we model the RF drive as a resonant series RLC circuit and assume that the input noise is broad band, then

$$S_V(\Omega \pm \omega_y) = \frac{S_V(\Omega)}{Q^2\left(1 - \left(1 \pm \frac{\omega_y}{\Omega}\right)^2\right)^2 + \left(1 \pm \frac{\omega_y}{\Omega}\right)^4} \ . \tag{53}$$

We have measured the output noise of a helical resonator with $Q = 290$ and $\Omega = 2\pi \times 30$ MHz driven by an RF amplifier at its resonant frequency in our laboratory and found it to be $S_V(\Omega) = 2.79 \times 10^{-14}$ V$^2$/Hz. Putting this all together we find that the heating rate due to voltage noise on the RF drive near the resonant frequency is of the order of $\dot{n}_y = 0.2$ s$^{-1}$. This is quite small compared to the resistive thermal fluctuation heating rates found in Section 3.4. In conclusion, RF drive noise contributions to the heating should be negligible for the planar ion trap designs considered here.

## 5 Comparison with Experiments

Data from recent ion trap experiments is shown in Fig. 8 [2]. The heating rate (along the axial direction, which is the motional mode used for most two qubit logic gates) is plotted as a function of trap size for experiments done with several different ion species, along with a dotted

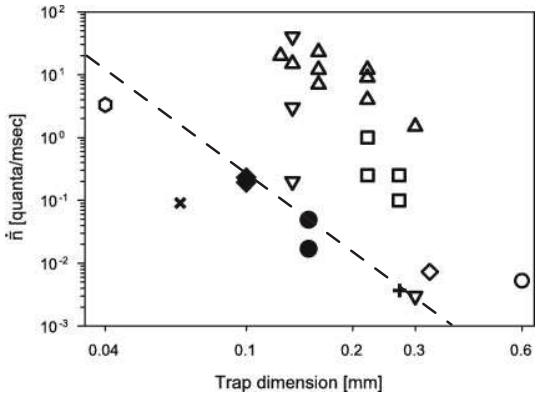


Fig. 8. Experimental ion heating rates, $\dot{n}$, as a function of distance of the ion from the nearest electrode, $d$. This data is taken from many experiments in different labs using different ion species; namely $^{111}Cd^+$ (filled circles and diamonds), $^{9}Be^+$ (empty triangles and squares), $^{198}Hg^+$ (empty diamonds), $^{40}Ca^+$ (empty circles), and $^{137}Ba^+$ (empty hexagons). The dashed line is a $d^{-4}$ guide to the eye indicating the scaling behavior of patch potential heating. Figure courtesy of L. Deslauriers, University of Michigan. We have overlaid our thermal noise heating estimate for the two-level trap described in Section 3.3 (+) and for the planar traps described in Section 3.4 (×).

line which indicates the $d^{-4}$ scaling consistent with patch potential heating. Since thermal noise heating scales with $d^{-2}$, this data suggests that thermal noise is not the dominant source of heating in current experiments. In addition, the experimental heating rates are much larger than that which is predicted by thermal noise calculations.

Also shown on Fig. 8 are the thermal heating rates for the two-level and planar traps from Sections 3.3 and 3.4. For the two-level trap, the predicted thermal heating rate $\dot{n} = 3.8$ s$^{-1}$ while the experimental heating rate is 100 s$^{-1}$ [1]. While there is no experimental data for the planar ion trap design, the predicted thermal heating rate is $\dot{n} = 88$ s$^{-1}$; this fundamental lower limit to the heating is by itself comparable to the total heating rate in many experiments. It is clear that as traps evolve towards smaller and semiconductor based designs, thermal noise heating will become more important in experiments.

## 6 Conclusions

As trap dimensions are scaled down, heating from thermal noise potentials generated by resistive elements in the RF and control circuits begin to increase the ion heating rates to the range that will introduce significant decoherence into quantum gates. Our analysis for the planar ion traps shows that the ion heating induced by resistive elements in the control electrodes is a particular concern. Future designs will have to minimize resistance in the control electrodes as well as the associated switching and supply resistances. Resistivity of the material used to make the RF electrodes is also important for traps where the RF rails are long, as will be the case for a many qubit quantum computer. Noise from the RF source does not appear to play a major role in the traps considered here.

Planar traps can be designed to minimize resistive thermal fluctuation heating. Since the dominant heating source in current designs is the resistance in the control electrode voltage source, the gaps between adjacent control electrodes should be kept as far away from the ion

as possible. To reduce heating in the $x$ direction, the gap in the control electrodes parallel to the RF rails at $x = 0$ which is used to tilt the principal axes can be changed to two gaps under the RF rails at $x = \pm(s + w_{RF}/2)$. To reduce heating in the $z$ direction, control electrodes should be made as long in the $z$ direction as practical and perhaps the area between the RF rails should not be segmented. This, however, involves a tradeoff in that higher control voltages will be required as the control electrode gaps are moved further away from the ion.

Even though the thermal noise heating is a concern, it is probably more important to understand and reduce the anomalous heating observed in experiments studied to date. Scaling the anomalous heating rates reported by [1] and [2] to the dimensions, secular frequencies, and ion masses used to calculate the resistive thermal fluctuation heating rates for planar traps in Section 3.4, the anomalous heating rates in planar traps would be of the order of $\dot{n} \sim 10^4$ s$^{-1}$. This estimate assumes that the anomalous heating rate scales as $d^{-4}$ where $d$ is the distance from the ion to the nearest trap electrode, as would be the case for patch potentials. This corresponds to a motional decoherence time of tens of microseconds which is only marginally longer than the time for a two qubit gate. Clearly there needs to be more research on the anomalous heating in order to make progress towards scaling down ion trap dimensions.

**Acknowledgements**

This work was supported in part by the Disruptive Technology Office (DTO) under the Department of Interior, NBC Acquisition and Property Mgmt Division, contract number NBC HC050151.

**References**

1. M.A. Rowe, A. Ben-Kish, B. DeMarco, D. Leibfried, V. Meyer, J. Beall, J. Britton, J. Hughes, W.M. Itano, B. Jelenkovic, C. Langer, T. Rosenband, and D.J. Wineland (2002), *Transport of quantum states and separation of ions in a dual RF ion trap*, Quantum Inf. Comput., Vol. 2, pp. 257–271.
2. L. Deslauriers, P.C. Haljan, P.J. Lee, K-A. Brickman, B.B. Blinov, M.J. Madsen, and C. Monroe (2004), *Zero-point cooling and low heating of trapped $^{111}Cd^{+}$ ions*, Phys. Rev. A, Vol. 70, pp. 043408.
3. Q.A. Turchette, D. Kielpinski, B.E. King, D. Leibfried, D.M. Meekhof, C.J. Myatt, M.A. Rowe, C.A. Sackett, C.S. Wood, W.M. Itano, C. Monroe, and D.J. Wineland (2000), Phys. Rev. A, Vol. 61, pp. 063418.
4. J. Chiaverini, R.B. Blakestad, J. Britton, J.D. Jost, C. Langer, D. Leibfried, R. Ozeri, and D.J. Wineland (2005), *Surface-electrode architecture for ion-trap quantum information processing*, Quantum Inf. Comput., Vol. 5, pp. 419–439.
5. C.E. Pearson, D.R. Leibrandt, W.S. Bakr, W.J. Mallard, K.R. Brown, and I.L. Chuang (2006), *Experimental investigation of planar ion traps*, Phys. Rev. A, Vol. 73, pp. 032307.
6. S. Seidelin, J. Chiaverini, R. Reichle, J.J. Bollinger, D. Leibfried, J. Britton, J.H. Wesenberg, R.B. Blakestad, R.J. Epstein, D.B. Hume, W.M. Itano, J.D. Jost, C. Langer, R. Ozeri, N. Shiga, D.J. Wineland (2006), *Microfabricated surface-electrode ion trap for scalable quantum information processing*, Phys. Rev. Lett., Vol. 96, pp. 253003.
7. D. Kielpinski, C. Monroe, and D.J. Wineland (2002), *Architecture for a large-scale ion-trap quantum computer*, Nature, Vol. 417, pp. 709–711.
8. J. Kim, S. Pau, Z. Ma, H.R. McLellan, J.V. Gates, A. Kornblit, and R.E. Slusher (2005), *System design for large-scale ion trap quantum information processor*, Quantum Inf. Comput., Vol. 5,

pp. 515–537.
9. D.J. Wineland, C. Monroe, W.M. Itano, B.E. King, D. Leibfried, D.M. Meekhof, C. Myatt, and C. Wood (1998), *Experimental primer on the trapped ion quantum computer*, Fortschr. Phys., Vol. 46, pp. 363–390.
10. T.A. Savard, K.M. O'Hara, and J.E. Thomas (1997), *Laser-noise-induced heating in far-off resonance optical traps*, Phys. Rev. A, Vol. 56, pp. R1095–R1098.
11. H.B. Callen and T.A. Welton (1951), *Irreversibility and generalized noise*, Phys. Rev., Vol. 83, pp. 34–40.
12. C. Henkel, S. Pötting, and M. Wilkens (1999), *Loss and heating of particles in small and noisy traps*, Appl. Phys. B, Vol. 69, pp. 379–387.
13. W.W. Macalpine and R.O. Schildknecht (1959), *Coaxial resonators with helical inner conductors*, Proc. IRE, Vol. 47, pp. 2099–2105.
14. J.R. Fisk (1976), *Helical-resonator design techniques*, QST, June, pp. 11–14.
15. B. Yurke and J.S. Denker (1984), *Quantum network theory*, Phys. Rev. A, Vol. 29, pp. 1419–1437.